RSC Advances

PAPER

View Article Online
View Journal | View Issue

Cite this: *RSC Adv.*, 2024, **14**, 19322

Magnetized cubic zinc MOFs for efficient removal of hazardous cationic and anionic dyes in aqueous solutions†

Ramy R. Abd El-Mouhsen,[a] Gamal O. El-Sayed,[b] Hesham H. El-Feky,[b] Mostafa M. H. Khalil *[a] and Islam M. El-Sewify *[a]

A significant amount of dye runoff and aqueous waste are released from the manufacturing process of dyes with intense and permanent colors, which are undesirable from a cultural and ecological aspect. In this paper, we present a green, simple, low-effort, and energy-efficient method of creating magnetized cubic Zn-MOFs for the adsorption and elimination of various organic dyes. Magnetic iron oxide materials with a hierarchical structure were loaded and doped into cubic zinc metal–organic frameworks (MDLZ). High magnetic characteristics, chemical stability, minimal toxicity, and ease of removing various dyes from aqueous effluents are all exhibited by the developed MDLZ adsorbent. To assess MDLZ's capacity to adsorb organic dyes from an aqueous solution, organic dyes such as Crystal Violet (CV), Neutral Red (NR), and Congo Red (CR) were used as model materials. Many adsorption factors were examined, including temperature, pH, contact time, initial concentration, and adsorbent dosage. Under optimal elimination circumstances, MDLZ was utilized to evaluate the kinetic, thermodynamic, and isotherm models for the adsorption of CR, NR, and CV dyes. The adsorption capacity (q_m) of the MDLZ adsorbent at 25 °C was 39.37 mg g^{-1} for CV, 239.81 mg g^{-1} for CR, and 321.54 mg g^{-1} for NR, which is significantly higher than those of other adsorbents reported. The magnetized nanocubes' large surface area and uniform micropores enabled them to eliminate a large number of organic dyes from wastewater effectively, and their strong adsorption capability persisted even after four reuse cycles. The microporous MLDZ adsorbent offers a simple and effective method for handling industrial effluents and filtration of water.

Received 1st April 2024
Accepted 7th June 2024

DOI: 10.1039/d4ra02453b

rsc.li/rsc-advances

Introduction

Dyes are organic molecules made up of chromophores. There are several varieties of dyes, which are classed as acidic, basic, or neutral depending on their application. Acidic dyes are water-soluble salts containing sulfuric, carboxylic, or phenolic groups that can be partially or completely bonded to cationic substrates such as wool, silk, nylon, and acrylic fibers. However, basic dyes are cationic dyes made up of azine, diazoic, and monoazoic chemicals.[1]

A significant amount of dyes are carcinogenic, teratogenic, or toxic, in addition to being physiologically hazardous.[2,3] The process of dyeing produces enormous amounts of wastewater containing dyes that are visually and ecologically unsatisfactory due to their intense, permanent color and high BOD (biological oxygen demand) loading.[4] The accumulation of cationic, anionic, and neutral dyes that commonly used in industry can certainly reduce the permeability of light into water bodies, resulting in a loss of photosynthesis and oxygen stock, compromising aquatic life.[5] The individual dye and its chemical characteristics, together with variables like exposure time, intensity, and sensitivity, can all have a significant impact on the health hazards connected with dyes. These carcinogenic dyes may raise the chance of acquiring cancer, especially in workplaces with high levels of exposure. As a result, in recent years, the elimination of dyes from water systems has received more attention. Various processes have been proposed to remove color pollution from contaminated water. Because they are too stable, traditional physicochemical and biological treatment techniques cannot effectively remove dye.[6] However, the main technologies employed for wastewater treatment in the textile industry involve membrane processes, ion exchange,[7] coagulation,[8] and adsorption.[9] One of the best methods for eliminating colors from aqueous solutions is a well-known separation technique called adsorption.[10,11] Because of its many benefits, including low cost, abundant supply of adsorbents, high adsorption capacity, simple regeneration potential, low energy consumption, and insensitivity to harmful contaminants, adsorption has a long track record and will likely remain popular.[12,13] Therefore, it is important to select appropriate

[a]Department of Chemistry, Faculty of Science, Ain Shams University, 11566, Abbassia, Cairo, Egypt. E-mail: eslamelsewify@sci.asu.edu.eg; khalil62@yahoo.com
[b]Department of Chemistry, Faculty of Science, Benha University, Egypt

† Electronic supplementary information (ESI) available. See DOI: https://doi.org/10.1039/d4ra02453b

adsorbing substances to remove different harmful pollutants. Several porous materials like activated carbons,[14] mesoporous materials,[15] zeolites,[16] and MOF[17–19] have been developed and employed for the adsorption elimination of toxicants. Porosity and suitable adsorbing sites on the substrate material are crucial for the efficient removal of contaminants. For the selective and effective removal of pollutants, certain active species, such as multiple functional groups (basic or acidic), metal salts, and their oxides and ions, are often inserted into the porous adsorbing materials.[20] Metal–organic frameworks (MOFs) shown distinct chemical functionalities that are useful for the selective capture of particular species, and these features are one of the attractive characteristics of MOFs.[21] MOF have a great deal of promise as adsorbents for eliminating of various contaminants, including hazardous gases, volatile organic compounds, inorganic pollutants such as heavy metals and radioactive metals, and organic contamination such as dyes, medicines, and pesticides.[22] MOFs used in dye removal processes to adsorb and extract dye molecules from water or wastewater.[23] Several interactions, including as hydrogen bonds, van der Waals forces, and electrostatic forces, can be used to explain the MOFs adsorption process for dye removal.[23] Magnetic adsorbent can be easily separated from solution after adsorption process. It's ability to reduce the high cost of isolation and extraction techniques that have been used in this filed due to their cost-effective recovery. The combination of magnetic nanoparticles and MOFs results in the formation of magnetic framework composites which combine advantages of both materials. In this paper, we present an easy and environmentally friendly method of creating magnetized cubic zinc MOFs for the removal of both anionic and cationic organic dyes as shown in Scheme 1. Magnetic iron oxide materials with a hierarchical structure were loaded and doped into cubic zinc organic frameworks (MDLZ). To assess the adsorption capacity of MDLZ from an aqueous solution, organic dyes including Congo Red (CR), Neutral Red (NR), and Crystal Violet (CV) were used as example agents. Several adsorption parameters, such as pH, contact duration, initial concentration, dose of the adsorbent, and temperature were investigated. MDLZ was used to assess the thermodynamic, isotherms, and kinetic models for the adsorption of CR, NR, and CV dyes under ideal removal parameters. Several organic dyes could be effectively removed form wastewater owing to the magnetized nanocubes' wide surface area and consistent microporous structure, which allowed for high adsorption capacity that lasted through several reuse cycles. The microporous MLDZ adsorbent offers an easy-to-use and efficient solution to control industrial wastewater and water purification.

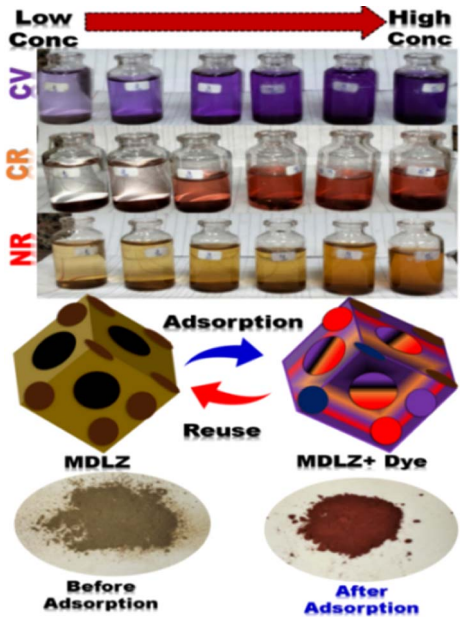

Scheme 1 The interactions between magnetite loaded and doped into cubic zinc metal–organic frameworks (MDLZ) adsorbent with CV, CR, and NR dye were examined at optimal conditions. The MDLZ adsorbent color changed from pale brown to reddish brown color, indicating the removal of the multiple dyes.

Results and discussion

Fabrication of nanocubic MDLZ adsorbent

The magnetite doped and loaded Zn-MOFs (MDLZ) were fabricated using a green and simple approach. During the preparation of Zn-MOF, the Zn nodes were mixed with 2-methylimidazole in presence of magnetite as shown in Scheme 2. To improve the adsorption characteristic of Zn-MOFs, the cubic Zn-MOFs were doped with the previously prepared magnetite (Fe_3O_4) to design magnetite doped nanocubes (MDZ). To enhance the magnetic properties of the MDZ, further loading process were done with polymerized magnetite using polyacrylamide (Fe_3O_4@PAM). FESEM Images investigate the preparation of nanocubes structures of Zn-MOFs which are randomly connected to create the microporous caves as shown in (Fig. 1A and B). Moreover, the aggregated nanospheres of the prepared Fe_3O_4 and Fe_3O_4@PAM images were demonstrated as shown in (Fig. 1C and D) respectively. Fig. 1E shows that the Fe_3O_4 was doped into nanocubes Zn-MOFs (MDZ). Moreover,

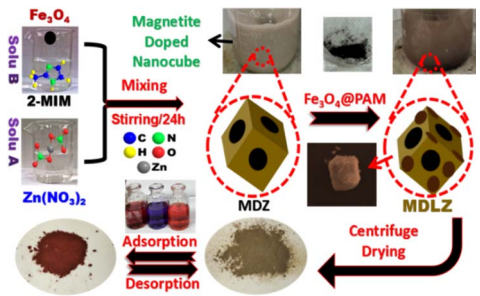

Scheme 2 The preparation of magnetite loaded and doped with into cubic zinc metal–organic frameworks (MDLZ) adsorbent *via* mixing of zinc nitrate salt with magnetite and 2-methylimidazole as a linker. The brown precipitate of MDLZ was observed after mixing and stirring for 24 h. The brown powder were separated, cleaned, and dried. The obtained MDLZ nanocubes were utilized in removal of CV, CR, and NR dyes.

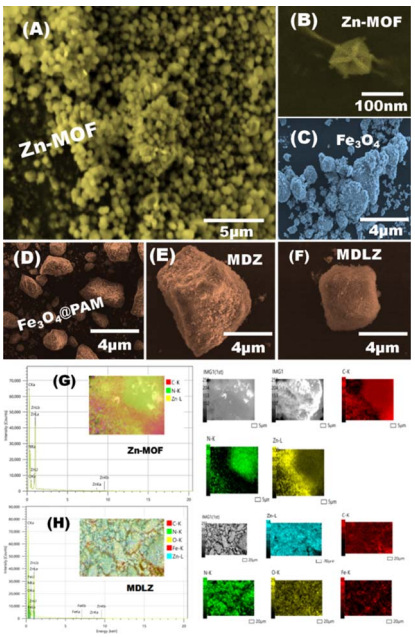

Fig. 1 Low- and high-magnification FESEM images of (A, B) the nanocube Zn-MOFs as intergrowing crystals, (C) Fe_3O_4, (D) Fe_3O_4@PAM, (E) MDZ and (F) cubic MDLZ adsorbent. FESEM-mapping of (G) Zn-MOFs and (H) MDLZ adsorbent.

our finding shows that the cubic morphology of the prepared Zn-MOFs platform was totally covered with Fe_3O_4@PAM to create bulk rock like morphology for capturing/trapping of multiple dyes from aqueous solution as shown in Fig. 1F. The FESEM mapping were utilized to demonstrate the distribution of magnetite into Zn-MOFs. Our results confirm the existence of Zn, C, and N elements of Zn-MOFs as shown in Fig. 1G.

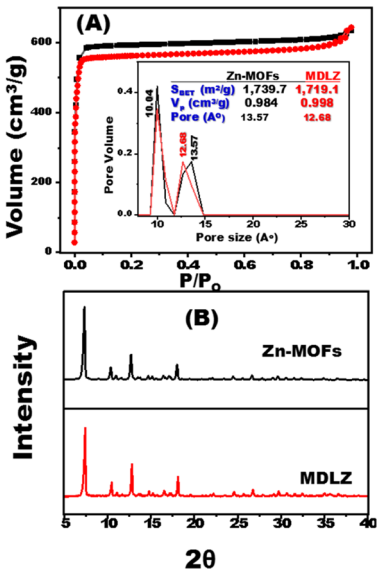

Fig. 2 (A) N_2 adsorption/desorption isotherms and (inset) BJH pore size distribution of the ZN-MOF and MDLZ. (B) Wide-angle XRD diffraction patterns of the ZN-MOF and MDLZ nanocubes.

Moreover, the distribution of Fe and O elements over the designed Zn-MOFs were confirmed as shown in Fig. 1H.

N_2 adsorption/desorption isotherms were designed to calculate the distribution of pore volume and surface area of the Zn-MOFs and MDLZ adsorbents (Fig. 2A).[24,25] Our findings demonstrate the manufacture of MDLZ adsorbents exhibiting homogeneous microporous voids. The adsorption/desorption isotherms' type I behavior, which is characterized by their sharpness, enables the building of microcage frameworks with pore sizes less than two nanometers. According to our studies, the pore size afterwards magnetite loading (12.68 Å) is slightly smaller than the parent (13.57 Å), as Fig. 2A shows. Our results demonstrated a remarkable decrease in Zn-MOFs surface area after loading of magnetite. The calculated surface area of the MDLZ was (1719 m^2 g^{-1}), which is lower than that of pure Zn-MOFs (1739.7 m^2 g^{-1}). Results further revealed the decoration of magnetite around the nanocubes and inside their microporous cages, thus illustrating the uniform filling of the microporous cavities of the inorganic–organic Zn-MOFs. The X-ray diffraction patterns for the Fe_3O_4 and Fe_3O_4@PAM were investigated as shown in Fig. S1A.† To clarify the crystal structure of Zn-MOFs and MDLZ adsorbents, X-ray diffraction patterns of the Zn-MOFs, MDLZ, MDZ were analyzed as shown in Fig. 2B and S2A.† The manufactured MDZ, MDLZ and Zn-MOFs show a sharp diffraction at 2θ of 7.33°, 10.30°, 12.77°, 16.41°, and 24.50° corresponded to the (211), (200), (220), and (222) planes, respectively. The finely resolved Bragg diffraction peaks of these two adsorbents show that they are highly crystalline and that uniform crystal structures are being formed.[26] Our findings further show that the nanocubes' diffraction peaks remain when magnetite is loaded and doped, indicating the utmost stability of their crystal structure. The FTIR spectra of Fe_3O_4 and Fe_3O_4@PAM were investigated as shown in Fig. S1B.† Moreover, the FTIR spectra for MDZ, Zn-MOFs, and MDLZ analyzed, as indicated in Fig. S2B and S3A† respectively, to gain insights into the surface function of the Zn-MOFs, MDZ and MDLZ adsorbents. The imidazole group's aromatic and aliphatic C–H absorption bands were measured at 2935 and 3130 cm^{-1} as shown in Fig. S2B and S3B† respectively. The 2-methyl imidazole C=N stretching mode absorption band was detected at 1580 cm^{-1}. The stretching bands of Zn–N and C–N were found at 420 cm^{-1} and within the 1460–1143 cm^{-1} area, respectively.[27]

Removal of dye using the MDLZ nanocubes

The best circumstances for removing CV, CR, and NR dyes from MDLZ adsorbent were examined. Changes in pH are predicted to have an impact on the adsorption of dye because the degree of ionization and surface charge of the adsorbent can be influenced by the pH of solute ions.[28,29] The CV, CR, and NR solutions' pH values were adjusted from 2 to 12. Fig. 3A illustrates the investigation of the pH's influence on the dye in CV, CR, and NR solutions following the adsorption procedure. According to our findings, the adsorption efficiency did not significantly improve as pH increased, and Fig. 3A illustrates that the greatest efficiency was observed at a neutral medium. Fig. 3B exhibits the results of a study into the impact of contact time, which ranged from 10 to

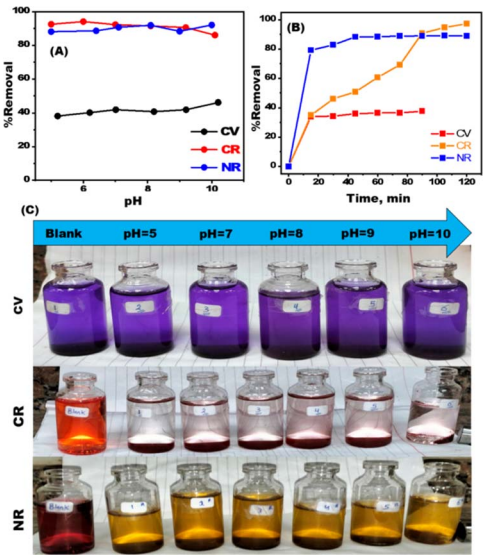

Fig. 3 (A) Effect of pH on CV, CR, and NR dye adsorption on MDLZ at room temperature. (B) The effect of time on the adsorption of MDLZ of different dyes under optimum conditions. (C) The corresponding images of MDLZ with CV, CR, and NR dyes at different dyes.

120 minutes, on removing of CV, CR, and NR dyes. According to our findings, the amount of dye removed by CV, CR, and NR became continuously with time until it achieved equilibrium. Our results demonstrated that the elimination of dye improved over time and reached saturation after 120 minutes. Our findings show that the presence of active centers and the wide surface area of MDLZ nanocubes contribute to an exceptionally high dye adsorption rate during the first hour of adsorption. The MDLZ's pores and active sites eventually became exhausted, which caused the dye adsorption rate to stabilize.[30] To identify the optimum dose of MDLZ, the adsorption experiments were conducted using 25 mg L^{-1} of CV, 125 mg L^{-1} of CR, and 50 mg L^{-1} NR at neutral medium and 298 K.

Our finding revealed that the adsorption capacity increased with increasing MDLZ dose, as shown in Fig. 4A. The performance of the MDLZ adsorbent may be significantly affected by the initial concentration of organic dyes, therefore the initial concentrations of CV, CR, and NR dyes were changed, and adsorption was carried out under suitable adsorption conditions (Fig. 4B). The initial concentrations were adjusted from 5 mg L^{-1} to 50 mg L^{-1} for the removal of CV under optimal conditions (25 mg dosage, 298 K temperature, and pH 7), as shown in Fig. 3B-a. According to our studies, removal efficiency decreased from 56.88% to 34.43%. As dye concentration increased. In addition, as Fig. 4B-b illustrates, the initial concentrations for CR removal were changed from 25 mg L^{-1} to 150 mg L^{-1} under specific conditions (a 25 mg dosage, 298 K temperature, and pH 6). Our findings demonstrated significant decrease in removal percentage from 98.61% to 37.88% as the dye concentration increased. As shown in Fig. 4B-c, the initial concentrations for NR removal were varied form 10 mg L^{-1} to 100 mg L^{-1} under optimum adsorption conditions (dose of 125 mg, temperature of 298 K, and pH 6). The results showed decrease in removal percentage from 90.1% to 75.99% as the dye concentration increased. This observation could be explained by the fact that MDLZ's binding sites have reached saturation, leaving insufficient active sites to capture all of the contaminating molecules in the solution.[31]

The surface charge of the MLDZ magnetic nanocubes adsorbent was investigated by examining the point of zero charge (PZC). Fig. S4† shows the PZCs of the MDLZ adsorbent at different pH values. Our findings indicated that the adsorbent's pH_{PZC} is 8.2, which is an essential variable in the removal of various dyes. The maximum adsorption capacity for cationic dyes was determined below the pH_{PZC}, whereas the functional groups of the MDLZ nanocubes adsorbent were protonated above the pH_{PZC}. Anionic dyes may be removed attributed to the MDLZ adsorbent surface's positive charge above the pH_{PZC}.[32] The Freundlich, Temkin, and Langmuir models are depicted as

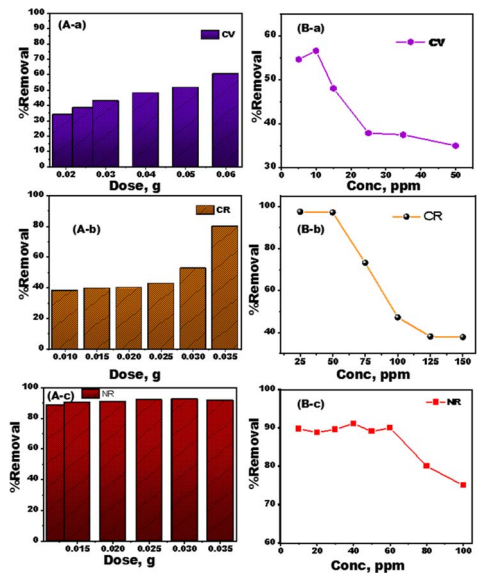

Fig. 4 (A) Effect of MDLZ nanocubes dosage on the adsorption capacity of the material for removal of (A-a) CV, (A-b) CR, and (A-c) NR dyes. (B) Effect of initial concentration of (B-a) CV, (B-b) CR, and (B-c) NR dyes at optimal conditions.

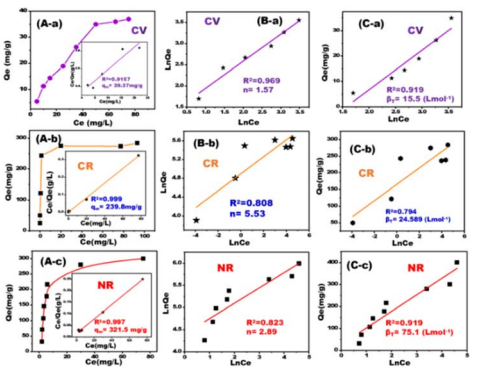

Fig. 5 (A) Adsorption isotherms of MDLZ for removal of (A-a) CV, (A-b) CR, and (A-c) NR dyes. (inset) Linear plot of the Langmuir isotherm curve. (B) Linear plot of the Freundlich adsorption isotherm. (C) Linear plot of the Temkin adsorption isotherm.

Table 1 Isotherms and their linear forms for the adsorption of different dyes

Isotherm	Value of parameters	CR	CV	NR
Langmuir	$q_{m\ exp}$	239.808	39.370	321.543
	K_L	4.38918	0.075505	0.197335
	R^2	0.999	0.9157	0.997
Freundlich	n	5.52	1.57	2.89
	K_F	133.92	3.69	81.8656
	R^2	0.8077	0.969	0.823
Temkin	β_T	24.589	15.532	75.0769
	K_T	839.398	0.2091	1.44
	R^2	0.794	0.9196	0.919

nonlinear and linear isotherm models, and their parameters were determined for the adsorption of CR, NR, and CV dyes at ambient temperature using MDLZ adsorbent (Fig. 5A).[33–35] At room temperature, the maximum adsorption capacity and Langmuir isotherm constant were determined by calculating the slope and intercept of the Langmuir plot of C_e/q_e against C_e (inset Fig. 5A). The Langmuir isotherm was shown to be more appropriate for interpreting the experimental results on the monolayer adsorption of dyes such as NR, CR, and CV when assessing the magnitude of R^2 (Fig. 5A). Furthermore, the high KL values observed served as confirmation of the dye's powerful adsorption and binding to the nanocubes cavities. Unfavorable deviations were found when the data were compared to the Freundlich isotherm (Fig. 5B) and Temkin isotherm (Fig. 5C) models. Table 1 summarizes the characteristics of all isotherms for the removal of various dyes. The MDLZ adsorbent exhibited a considerably greater adsorption capacity (q_m) for CV (39.37 mg g^{-1}), CR (239.81 mg g^{-1}), and NR (321.54 mg g^{-1}) at 25 °C when compared to other adsorbents listed in Table 2.[36–60]

As shown in Fig. 6, the adsorption rate of the MDLZ adsorbent was investigated to clarify the kinetics of the uptake of NR, CR, and CV dyes. Adsorption of cationic and anionic dyes onto the MDLZ nanocubes adsorbent initiated at a high rate and decreased gradually until equilibrium was attained. After 100 minutes, there was an evident rise in both the removal rate and highest adsorption, and this consequently was determined to be the equilibrium time. The removal approach's kinetics are a crucial parameter for evaluating adsorption dynamics. The adsorption kinetics of CV, CR, and NR dyes onto MDLZ were assessed by fitting the experimental data with the pseudo-first order and pseudo-second order models. The adsorption capacity at equilibrium, q_e (cal) was identified by using the slope and intercept of $\log(q_e - q_t)$ *vs.* t plots (Fig. 6A), which were utilized to determine the rate constant, K_1. The results suggest that the kinetics of dye adsorption for CV, CR, and NR dyes

Table 2 Comparison of adsorption of proposed work and others

Dye	Adsorbent	Adsorption capability (mg g^{-1})	Ref.
CR	Chitosan/TiO_2	32	36
	Cellulose/Fe_3O_4/activated carbon composite	66	37
	Interconnected polypyrrole–polyaniline nanofibres	222	38
	Activated bentonites	7	39
	Fe_3O_4/NiO	89.9	40
	ZnO	208	41
	Activated carbon	300	42
	Co-doped ZnO	230	43
	Mn-doped ZnO	232.5	44
	MDLZ	**239.808**	**Our work**
NR	Chitosan	16.75	45
	Activated carbon chitosan	36.20	45
	rGO/SiO_2 nanocomposites	66.635	46
	$Zn_3[Co(CN)_6]_2 \cdot nH_2O$ nanospheres	24.06	47
	Fe_3O_4 hollow nanospheres	29.5	48
	Bentonite/carbon composites	46	49
	$Ni_{0.5}Zn_{0.5}Fe_2O_4/SiO_2$ nanocomposites	39.95	50
	Halloysite nanotubes	65.45	51
	WFS	232.5	51
	Cottonseed hull substrate	166.7	52
	CuO_NP	283	53
	Pleurotus ostreatus nanoparticles (PONS)	61.73	54
	MDLZ	**321.543**	**Our work**
CV	BC-PKS	24.45	55
	Himalayan long-leaf pine bark	32.78	56
	Magnetite nanoparticles loaded onto Azolla	30.21	57
	Nanomagnetic iron oxide	16.5	58
	Magnetically modified activated carbon	67.1	58
	AC – from date palm leaflets	36.63	59
	Activated carbon of Lemon Wood (ACL)	23.6	60
	Activated carbon/Fe_3O_4	35.64	60
	MDLZ	**39.370**	**Our work**

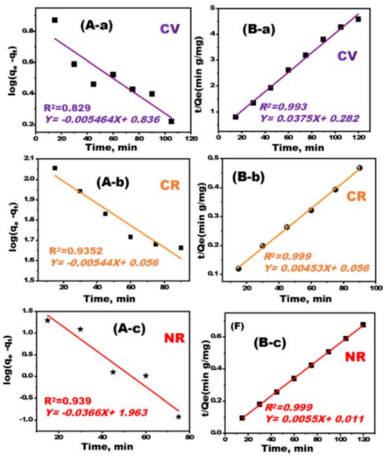

Fig. 6 Determination of the adsorption kinetics of (A-a) CV, (A-b) CR, and (A-c) NR dyes onto MDLZ *via* the pseudo-first order and pseudo-second order of (B-a) CV, (B-b) CR, and (B-c) NR dyes onto adsorption models at room temperature.

follow the pseudo-second-order kinetic model. The correlation coefficients calculated with the pseudo-first-order kinetic model were lower than those achieved using the pseudo-second-order kinetic model (Fig. 6B). The correlation coefficients and q_e (calc.) values from the pseudo-second-order kinetic model are in agreement with the results that has been obtained (Table 3). Our findings showed that the rate-limiting step of the adsorption process is chemisorption, which involves strong forces *via* the exchange or sharing of electrons between the multifunctional surface of MDLZ and CV, CR, and NR dyes adsorption molecules.

The influence of temperature on adsorption must be investigated for practical adsorbent uses. Three different temperatures were used for adsorption experiments: 25 °C, 40 °C, and 60 °C and the thermodynamic parameters were determined as shown in Table 4. The adsorption capacity of the MDLZ nanocubes for removal of CR increased as the temperature increased from 25 °C to 60 °C, demonstrating endothermic CR adsorption onto the nanocubic MDLZ adsorbent (Fig. S5A & B†). Our findings could be explained by the fact that when temperature increases, the dye molecules' mobility and diffusion rate over the adsorbent's surface increase, enhancing the adsorbent's capacity for adsorption,[61,62] Table 4 shows the results of the calculation of the appropriate thermodynamic parameters. The adsorption process is confirmed to be endothermic by the positive value of ΔH°; the process of adsorption of CR dye is demonstrated to be spontaneous by the negative value of ΔG°. The reaction's feasibility is confirmed to increase with temperature by the increasing negativity of ΔG°; and the system's disorder increases after dye adsorption by the positive value of ΔS°.[63,64] In contrast, the adsorption capacity of the MDLZ nanocubes for cationic dye such as CV and NR dyes decreased as the temperature increased from 25 °C to 60 °C, thus confirming the exothermic removal process of CR onto the MDLZ adsorbent (Fig. S5C and D†). The adsorption process of NR and CV dyes is exothermic, as demonstrated by the negative values of ΔH^{o} measured at three distinct temperatures. During the adsorption process, there could be a formation of chemical bonds or molecular organization reflected in the negative ΔS^{o} values.

The mechanism of adsorption using MDLZ nanocubes

Several parameters were taken into consideration when examining the potential adsorption mechanism of MDLZ of CV, CR, and NR dyes. Electrostatic interactions between MDLZ nanocubes and the cationic and anionic dyes have been demonstrated to be one of the primary adsorption processes. In order to identify the alterations in various functional groups and peak locations after adsorption of organic dyes, the SEM, XRD and FTIR analysis were performed as shown in Fig. 7. Our SEM images investigate the accumulation of organic dyes over the nanocubes as shown in Fig. 7A. Our findings further show that the nanocubes' diffraction peaks remain when the organic dyes adsorption, indicating the utmost stability of MDLZ adsorbents Fig. 7B. Furthermore, π–π interactions contribute to the organic dyes CV, CR, and NR's capture process, which amplifies the adsorption impact. The remarkable performance of MDLZ nanocubes in dye removal can be attributed to the combined action of hydrogen bonding, electrostatic interactions, and π–π interactions during the adsorption process of dyes such as CV, CR, and NR. The intraparticle diffusion mechanism of the MDLZ adsorbent for the removal of CV, CR, and NR dyes was investigated from the slope of the corresponding second linear region (Fig. S6†). Our findings suggested that the early phases of adsorption regulated the mass transfer resistance to the dye particles of CV, CR, and NR dyes. Thus, the pseudo-second-order kinetic model may be used to estimate the adsorption kinetics. Chemisorption through the sharing or exchange of electrons between the multifunctional surfaces of MDLZ and the dyes CV, CR, and NR appeared to be the rate-limiting process. The spontaneous interactions between the cationic

Table 3 Kinetic parameters and their correlation coefficients for the adsorption process

Model	Parameters	CR	CV	NR
Pseudo-first-order kinetic	K_1 (min^{-1})	0.0124362	0.012583592	0.084289
	q_e (mg g^{-1})	125.9795347	6.854882265	91.7698
	R^2	0.9352	0.836	0.9397
Pseudo-second-order kinetic	K_2	0.00036	0.004986702	0.002700
	q_e	222.22	26.67	181.82
	R^2	0.999	0.993	0.9998
Experimental data	q_e (exp)	239.81	39.370	321.543

Table 4 Standard enthalpy, entropy, and free energy changes for CR, CV, and NR adsorption on MDLZ

Dye	(Conc) (ppm)	ΔH^o	ΔS^o	ΔG^o (kJ mol^{-1}) 293 K	313 K	333 K
CR	125	213.33	726.11	−2.79	−10.435	−16.58
CV	35	−18.79	55.6	−1.85	−0.838	−0.759
NR	50	−37.49	−89.79	−10.06	−8.62	−8.29

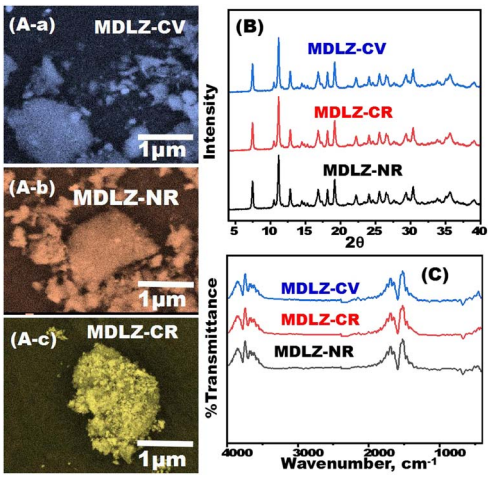

Fig. 7 (A) FESEM images of MDLZ after adsorption of (A-a) CV, (A-b) NR, and (A-c) CR dyes. (B) XRD diffraction patterns of the MDLZ nanocubes after adsorption of organic dyes. (C) The FTIR spectra of the nanocubes MDLZ after adsorption of organic dyes.

and anionic dyes could be responsible for the adsorption process.[65]

Reusability and applicability of nanocubes MDLZ

If adsorbent material can be utilized over several cycles and still be beneficial for recovery, separation, and dye removal after regeneration, it is assumed to be cost-effective. After elution in an aprotic and portic solvent solution, the separation (collection) of dyes collected by the nanocubes adsorbent was examined. After four successive adsorption–desorption cycles, we detected a shift in MDLZ's adsorption capability. The process of creating a pH shift is typically used to accomplish the desorption of cationic or anionic dyes. Desorption is often carried out in basic or acidic environments. In order to regenerate nanocubes dye-MDLZ, 0.02 g of the adsorbent was placed in a flask and repeatedly washed with a different solvent until all of the dye molecules had desorbed from the MDLZ surface. The adsorbent was then continuously cleaned with distilled water. Ethanol was used to remove the remaining dyes from the adsorbent. After collecting, the dye free adsorbent was subjected to heating to 60 °C for four hours. The subsequent dye adsorption experiment employed the dye free adsorbent after regeneration. The partial obstruction of MDLZ's adsorption sites is responsible for the little reduction in regeneration efficiency (Fig. S7†). In order to determine if MDLZ could be utilized for eliminating several dyes, three different concentrations of NR, CR, and CV dyes were combined under optimal conditions. As seen in (Fig. S8†), the findings suggested that the MDLZ adsorbent could trap or remove the three dyes. As a result, the produced MDLZ adsorbent has great promise for the removal of CV, CR, and NR dyes from modeled samples that include many cationic and anionic dyes. Our findings investigated the high removal percentage of organic dyes in comparison with Zn-MOFs, Fe_3O_4, and Fe_3O_4@PAM as shown in Fig. 8A. The designed MDLZ show ferromagnetic characteristic with considerable magnetic sustainability in comparison with Fe_3O_4, and Fe_3O_4@PAM as shown in Fig. 8B.

Experimental

Chemicals

The chemicals obtained for this research were used as received without further purification since they were of analytical grade. These chemicals included zinc nitrate hexahydrate (≥99.0%) [$Zn(NO_3)_2 \cdot 6H_2O$], 2-methylimidazole (2-MIM) which were purchased from Sigma-Aldrich. Ferrous sulfate heptahydrate [$FeSO_4 \cdot 7H_2O$]. Hexahydrated ferric chloride [$FeCl_3 \cdot 6H_2O$, m.wt (270.3 g mol^{-1})], acrylamide. ammonium peroxydisulfate [$(NH_4)_2S_2O_8$, ammonium hydroxide [NH_4OH, (25%)]. Congo red dye (99%), neutral red dye (99%) and crystal violet dye (99%). Milli-Q Water, methanol (99.7%), *N*,*N*-dimethylformamide anhydrous (99.8%), buffer solutions of KCl–HCl and CH_3-$COOH$–CH_3COONa were used to adjust the pH in the acidic medium. 4-(2-Hydroxyethyl)-1-piperazineethanesulfonic acid and 0.1 M disodium hydrogen phosphate were used to adjust the pH in the basic medium using 0.1 M NaOH. All chemicals were used directly as received without any purification.

Preparation of nanocubic MDLZ adsorbent

To prepare magnetite doped Zn-MOF, 3.672 g of $Zn(NO_3)_2 \cdot 6H_2O$ dissolved in 50 mL of methanol and 0.05 g Fe_3O_4 added then sonicated for 3 min, and 4.053 g of 2-MIM dissolved in 50 mL of methanol. The two solutions were mixed and stirred for 24 h at room temperature. The magnetite-doped Zn-MOF (MDZ) was

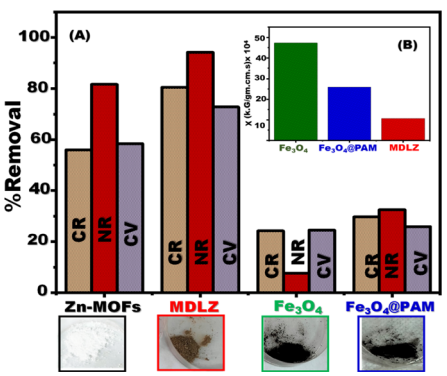

Fig. 8 (A) The comparison in removal percentage of CR, CV, and NR dyes using different adsorbents such as Zn-MOFs, MDLZ, Fe_3O_4, and Fe_3O_4@PAM under optimum adsorption conditions. (B) The magnetic susceptibility of MDLZ, Fe_3O_4, and Fe_3O_4@PAM.

formed and separated from the solution *via* centrifuge and washed with methanol and then dried for 24 h at 50 °C. To prepare MDLZ, 0.1 g of (MDZ) was suspended in to 25 mL of methanol and 0.05 g of Fe_3O_4@PAM was sonicated into 25 mL of methanol for 3 min. The two solutions were mixed and stirred for 24 h at room temperature. The obtained composite (MDLZ) was separated from the solution *via* centrifuge then washed by methanol and dried for 24 h at 50 °C.

Removal and batch studies of the MDLZ

Stock solutions of Congo red dye (CR), neutral red (NR) dye and crystal violet dye (CV) (1000 mg L^{-1}) were prepared to determine the optimal adsorption conditions. The working concentrations of the dye's solutions were prepared using the stock solution and varied from (25–125) mg L^{-1} for CR dye, from (10–60) mg L^{-1} for NR dye and from (5–35) mg L^{-1} for CV dye. Deionized water was used to prepare the stock solutions. The adsorption performance of MDLZ for different dyes removal was investigated by conducting multiple batch adsorption experiments. The required amount of MDLZ adsorbent was added to aqueous solutions with a constant concentration of dye. The mixture was then continually agitated on a shaker. At the end of predetermined time periods, an aliquot of the solution was removed, separated *via* centrifugation at 6000 rpm, and analyzed *via* UV-Vis spectroscopy. The complete description of instruments was discussed in detail in ESI.†

Conclusions

In this report, simple and energy-efficient protocol of creating magnetized cubic Zn-MOFs for the adsorption of different organic dyes. Cubic zinc metal–organic frameworks were loaded and doped with magnetic iron oxide materials that exhibited a hierarchical structure. The produced MDLZ has several notable characteristics, including high magnetic properties, chemical stability and ease of dye removal from aqueous effluents. The organic dyes including crystal violet (CV), neutral red (NR), and Congo red (CR) dyes were employed as model materials to evaluate MDLZ's ability to adsorb from an aqueous solution. Many adsorption factors were examined, including temperature, pH, contact duration, initial concentration, and adsorbent dosage. Thermodynamic, isothermal, and kinetic models for the adsorption of CR, NR, and CV dyes under optimal elimination conditions were evaluated using MDLZ adsorbents. The adsorption capacity of the MDLZ adsorbent at 25 °C for CV was 39.37 mg g^{-1}, for CR was 239.81 mg g^{-1}, and NR was 321.54 mg g^{-1} which is significantly higher than those of other adsorbents reported. Our findings showed that the rate-limiting step of the adsorption process is chemisorption, which involves strong forces *via* the exchange or sharing of electrons between the multifunctional surface of MDLZ and CV, CR, and NR dyes adsorption molecules. The ferromagnetic properties, large surface area and uniform micropores of the magnetized nanocubes allowed for eliminate an extensive amount of organic dyes from wastewater effectively, and their strong adsorption capability maintained even after multiple uses. The microporous MLDZ adsorbent offers a simple and effective method for controlling industrial wastewater and filtration of water.

Conflicts of interest

There are no conflicts to declare.

Notes and references

1 E. Natarajan and G. P. Ponnaiah, *Environ. Nanotechnol., Monit. Manage.*, 2017, **7**, 73–88.
2 H.-Y. Zhu, L. Xiao, R. Jiang, G.-M. Zeng and L. Liu, *Chem. Eng. J.*, 2011, **172**, 746–753.
3 N. M. Mahmoodi, *J. Ind. Eng. Chem.*, 2015, **27**, 251–259.
4 T. Wu, T. Lin, J. Zhao, H. Hidaka and N. Serpone, *Environ. Sci. Technol.*, 1999, **33**, 1379–1387.
5 A. A. Babaei, S. N. Alavi, M. Akbarifar, K. Ahmadi, A. Ramazanpour Esfahani and B. Kakavandi, *Desalin. Water Treat.*, 2016, **57**, 27199–27212.
6 A. Radwan, S. O. Mohamed, M. M. Khalil and I. M. El-Sewify, *Sci. Rep.*, 2024, **14**(1), 9061.
7 H. J. Gao, S. F. Wang, L. M. Fang, G. A. Sun, X. P. Chen, S. N. Tang, H. Yang, G. Z. Sun and D. F. Li, *Mater. Today Chem.*, 2021, **22**, 100593.
8 U. Habiba, T. A. Siddique, T. C. Joo, A. Salleh, B. C. Ang and A. M. Afifi, *Carbohydr. Polym.*, 2017, **157**, 1568–1576.
9 S. A. Hosseini, M. Vossoughi, N. M. Mahmoodi and M. Sadrzadeh, *J. Cleaner Prod.*, 2018, **183**, 1197–1206.
10 A. Bhatnagar and A. K. Jain, *J. Colloid Interface Sci.*, 2005, **281**, 49–55.
11 A. Özcan and A. S. Özcan, *J. Hard Mater.*, 2005, **125**, 252–259.
12 J. Chen, L. Liu, J. Huang, C. Sheng and L. Li, *Mater. Today Chem.*, 2022, **23**, 100661.
13 M. Habibi, S. Rafiaei, A. Alhaji and M. Zare, *J. Alloys Compd.*, 2022, **890**, 161901.
14 M. S. Reza, C. S. Yun, S. Afroze, N. Radenahmad, M. S. A. Bakar, R. Saidur, J. Taweekun and A. K. Azad, *Arab J. Basic Appl. Sci.*, 2020, **27**, 208–238.
15 N. Bensacia, I. Fechete, K. Boutemak and A. Kettab, *Environmental Footprints and Eco-Design of Products and Processes*, 2022, 169–186.
16 L. F. De Magalhães, G. R. Da Silva and A. E. C. Peres, *Adsorpt. Sci. Technol.*, 2022, 2022.
17 J. Ru, X. Wang, F. Wang, X. Cui, X. Du and X. Lu, *Ecotoxicol. Environ. Saf.*, 2021, **208**, 111577.
18 L. Huang, R. Shen and Q. Shuai, *J. Environ. Manage.*, 2021, **277**, 111389.
19 M. J. Uddin, R. E. Ampiaw and W. Lee, *Chemosphere*, 2021, **284**, 131314.
20 N. A. Khan, Z. Hasan and S. H. Jhung, *J. Hazard. Mater.*, 2013, **244–245**, 444–456.
21 R. M. Rego, G. Kuriya, M. D. Kurkuri and M. Kigga, *J. Hazard. Mater.*, 2021, **403**, 123605.
22 S. Soni, P. K. Bajpai, J. Mittal and C. Arora, *J. Mol. Liq.*, 2020, **314**, 113642.

23 I. M. El-Sewify and S. Ma, *Langmuir*, 2024, **40**(10), 5060–5076.
24 M. Y. Y. Emran, M. Mekawy, N. Akhtar, M. A. A. Shenashen, I. M. M. EL-Sewify, A. Faheem and S. A. A. El-Safty, *Biosens. Bioelectron.*, 2018, **100**, 122–131.
25 I. M. El-Sewify, M. A. Shenashen, R. F. El-Agamy, M. S. Selim, N. F. Alqahtani, A. Elmarakbi, M. Ebara, M. M. Selim, M. M. Khalil and S. A. El-Safty, *J. Hazard. Mater.*, 2024, **465**, 133271.
26 I. M. El-Sewify, A. Radwan, A. Shahat, M. F. El-Shahat and M. M. H. Khalil, *Microporous Mesoporous Mater.*, 2022, **329**, 111506.
27 C. L. Hobday, C. H. Woodall, M. J. Lennox, M. Frost, K. Kamenev, T. Düren, C. A. Morrison and S. A. Moggach, *Nat. Commun.*, 2018, **9**, 1–9.
28 Y. Zhang, C. Zhu, F. Liu, Y. Yuan, H. Wu and A. Li, *Sci. Total Environ.*, 2019, **646**, 265–279.
29 A. Gürses, K. Güneş and E. Şahin, *Green Chemistry and Water Remediation: Research and Applications*, 2021, 135–187.
30 E. Misran, O. Bani, E. M. Situmeang and A. S. Purba, *Alexandria Eng. J.*, 2022, **61**, 1946–1955.
31 S. Sultana, K. Islam, M. A. Hasan, H. M. J. Khan, M. A. R. Khan, A. Deb, M. Al Raihan and M. W. Rahman, *Environ. Nanotechnol., Monit. Manage.*, 2022, **17**, 100651.
32 S. Wong, H. H. Tumari, N. Ngadi, N. B. Mohamed, O. Hassan, R. Mat and N. A. Saidina Amin, *J. Cleaner Prod.*, 2019, **206**, 394–406.
33 I. Langmuir, *J. Am. Chem. Soc.*, 1917, **39**, 1848–1906.
34 H. Freundlich and W. Heller, *J. Am. Chem. Soc.*, 1939, **61**, 2228–2230.
35 *Recent modifications to Langmuir isotherms – ScienceOpen*, **https://www.scienceopen.com/document?vid=a5ad913b-eecc-42b0-bf4a-99eb46d86c75**, (accessed 28 March 2024).
36 U. Habiba, T. C. Joo, S. K. A. Shezan, R. Das, B. C. Ang and A. M. Afifi, *Desalin. Water Treat.*, 2019, **164**, 361–367.
37 H. Y. Zhu, Y. Q. Fu, R. Jiang, J. H. Jiang, L. Xiao, G. M. Zeng, S. L. Zhao and Y. Wang, *Chem. Eng. J.*, 2011, **173**, 494–502.
38 M. Bhaumik, R. McCrindle and A. Maity, *Chem. Eng. J.*, 2013, **228**, 506–515.
39 M. Toor, B. Jin, S. Dai and V. Vimonses, *J. Ind. Eng. Chem.*, 2015, **21**, 653–661.
40 P. Koohi, A. Rahbar-kelishami and H. Shayesteh, *Environ. Technol. Innovation*, 2021, **23**, 101559.
41 S. Chawla, H. Uppal, M. Yadav, N. Bahadur and N. Singh, *Ecotoxicol. Environ. Saf.*, 2017, **135**, 68–74.
42 M. K. Purkait, A. Maiti, S. DasGupta and S. De, *J. Hazard. Mater.*, 2007, **145**, 287–295.
43 S. Sachin, B. K. Pramanik, N. Singh, R. Zizhou, S. Houshyar, I. Cole and H. Yin, *Nanomaterials*, 2023, **13**, 566.
44 Sachin, N. Singh, K. Shah and B. K. Pramanik, *Environ. Res.*, 2023, **233**, 116484.
45 F. P. de Freitas, A. M. M. L. Carvalho, A. D. C. O. Carneiro, M. A. de Magalhães, M. F. Xisto and W. D. Canal, *Heliyon*, 2021, **7**, e07629.
46 J. Wang, T. Chen, B. Xu and Y. Chen, *Appl. Sci.*, 2020, **10**, 8529.
47 W. Wang, C. Li, J. Yao, B. Zhang, Y. Zhang and J. Liu, *J. Mol. Liq.*, 2013, **184**, 10–16.
48 M. Iram, C. Guo, Y. Guan, A. Ishfaq and H. Liu, *J. Hazard. Mater.*, 2010, **181**, 1039–1050.
49 N. Fathy, S. El-Khouly, S. Ahmed, T. El-Nabarawy and Y. Tao, *Asia-Pac. J. Chem. Eng.*, 2021, **16**, e2586.
50 R. Liu, H. Fu, Y. Lu, H. Yin, L. Yu, L. Ma and J. Han, *J. Nanosci. Nanotechnol.*, 2016, **16**, 8252–8262.
51 P. Luo, Y. Zhao, B. Zhang, J. Liu, Y. Yang and J. Liu, *Water Res.*, 2010, **44**, 1489–1497.
52 Q. Zhou, W. Gong, C. Xie, D. Yang, X. Ling, X. Yuan, S. Chen and X. Liu, *J. Hazard. Mater.*, 2011, **185**, 502–506.
53 T. B. Vidovix, E. F. D. Januário, M. F. Araújo, R. Bergamasco and A. M. S. Vieira, *Environ. Prog. Sustainable Energy*, 2022, **41**, e13864.
54 D. Y. Lei, B. Li, Q. Wang, B. Wu, L. Ma and H. Xu, *Desalin. Water Treat.*, 2015, **54**, 2794–2805.
55 P. P. Kyi, J. O. Quansah, C. G. Lee, J. K. Moon and S. J. Park, *Appl. Sci.*, 2020, **10**, 2251.
56 R. Ahmad, *J. Hazard. Mater.*, 2009, **171**, 767–773.
57 N. Alizadeh, S. Shariati and N. Besharati, *Int. J. Environ. Res.*, 2017, **11**, 197–206.
58 S. Hamidzadeh, M. Torabbeigi and S. J. Shahtaheri, *J. Environ. Health Sci. Eng.*, 2015, **13**, 1–7.
59 M. Sulyman, J. Namieśnik and A. Gierak, *Inżynieria iOchrona Środowiska*, 2016, **19**(4), 611–631.
60 R. Foroutan, S. J. Peighambardoust, S. H. Peighambardoust, M. Pateiro and J. M. Lorenzo, *Molecules*, 2021, **26**, 2241.
61 P. J. Jodłowski, G. Kurowski, K. Dymek, R. J. Jędrzejczyk, P. Jeleń, Kuterasiński, A. Gancarczyk, A. Węgrzynowicz, T. Sawoszczuk and M. Sitarz, *Microporous Mesoporous Mater.*, 2020, **303**, 110249.
62 P. J. Jodłowski, G. Kurowski, Ł. Kuterasiński, M. Sitarz, P. Jeleń, J. Jaśkowska, A. Kołodziej, A. Pajdak, Z. Majka and A. Boguszewska-Czubara, *ACS Appl. Mater. Interfaces*, 2021, **13**, 312–323.
63 T. Patra, A. Mohanty, L. Singh, S. Muduli, P. K. Parhi and T. R. Sahoo, *Chemosphere*, 2022, **288**, 132472.
64 A. Sharma, D. Mangla, A. Choudhry, M. Sajid and S. Ali Chaudhry, *J. Mol. Liq.*, 2022, **362**, 119752.
65 S. Koppula, P. Jagasia and S. B. M. Surya, *Mater. Today Commun.*, 2023, **34**, 105336.